Influence of well-width fluctuations on the binding energy of excitons, charged excitons, and biexcitons in GaAs-based quantum wells

A. V. Filinov,[1,2,3] C. Riva,[1] F. M. Peeters,[1] Yu. E. Lozovik,[2] and M. Bonitz[3]
[1]*Departement Natuurkunde, Universiteit Antwerpen (Drie Eiken Campus), Universiteitsplein 1, B-2610 Antwerpen, Belgium*
[2]*Institute of Spectroscopy RAS, Moscow region, Troisk 142190, Russia*
[3]*Christian-Albrechts-Universität zu Kiel, Institut für Theoretische Physik und Astrophysik, Leibnizstrasse 15, 24098 Kiel, Germany*
(Received 19 January 2004; revised manuscript received 8 April 2004; published 28 July 2004)

We present a first-principle path integral Monte Carlo (PIMC) study of the binding energy of excitons, trions (positively and negatively charged excitons) and biexcitons bound to single-island interface defects in quasi-two-dimensional $GaAs/Al_xGa_{1-x}As$ quantum wells. We discuss in detail the dependence of the binding energy on the size of the well-width fluctuations and on the quantum-well width. The numerical results for the well-width dependence of the exciton, trions and biexciton binding energy are in good quantitative agreement with the available experimental data.

DOI: 10.1103/PhysRevB.70.035323 PACS number(s): 71.35.Cc, 73.21.Fg, 71.35.−y, 71.23.An

I. INTRODUCTION

Excitonic atoms and molecules in quantum confined semiconductors have been intensively investigated in the last decade. These systems show nontrivial Coulomb correlation effects leading to interesting optical and transport characteristics not seen in bulk materials. A strong increase of the binding energy of the excitonic complexes was found experimentally[1–10] with decreasing quantum well (QW) width and increasing magnetic field.[11]

In the literature there has been an active discussion about the influence of localization potentials on the binding energy of excitons and excitonic complexes.[11] Most of the theoretical calculations[12–17] show a substantially weaker dependence of the binding energies on the QW width than those experimentally observed.[1,2,4–10] In particular, it was found experimentally that the binding energy of the charged excitonic complex is for narrow quantum wells much larger than the one estimated theoretically, the difference being typically a factor of two for narrow QWs. An explanation for this could be the trapping of the excitons (trions, biexcitons) by ionized donors in the barriers[18] or by some kind of interface defects produced by the mixture of well and barrier materials during the QW growth process, i.e., by QW width fluctuations or fluctuations in the alloy composition of the barrier, which were not taken into account in Refs. 12–17. Such effects can induce an additional weak lateral confinement which leads to the confinement of the particles in all three dimensions like in the case of a quantum dot potential. The low-temperature photoluminescence of such structures originates from the radiative recombination of the exciton states localized at such nonuniformities of the heterostructure potential. In this situation broadening and splittings of both exciton and trion peaks develops in the PL spectra.[19] Such lateral confinement becomes more important in narrow quantum wells. Theoretical calculations of exciton, trion, and biexciton states in such structures is a fairly complex problem because of the need to take simultaneous account of the Coulomb interaction and the three-dimensional heterostructure potential, which is no longer translationally invariant.

The standard theoretical approach to calculate binding energies is to solve the corresponding many-particle Schrödinger equation by means of an appropriate basis expansion. This works efficiently in simple geometries but is not easily applicable to our problem with well-width fluctuations. Recently, a different approach was developed which is based on solving the Bloch equation for the many-particle density matrix.[24] It was demonstrated in Ref. 24 that this problem can be efficiently solved using path integral Monte Carlo (PIMC) methods without any restrictions on the geometry of the confinement potential. No quantum well-width fluctuation effects were considered in Ref. 24.

The aim of the present paper is to understand and explain recent experimental data on the binding energy of the ground state excitons, trions, and biexcitons in QWs by including localization effects. We consider localization as a consequence of the local modulation of the thickness of the quantum well of 1–2 monolayers (ML) which corresponds to the experimental findings of Ref. 19. In agreement with experimental results, we find that such QW width fluctuations can increase the trion binding energy in GaAs-based quantum wells by up to 100% as compared to ideal QWs without interface roughness.

We also found that for lateral localization diameters exceeding $D \approx 150$ Å the binding energy of the negative trion can become larger than that of the positive trion, in contrast to the case of ideal QWs where the positively charged excitons are slightly more strongly coupled. The reason is that the localization confinement has a different influence on the lateral wave functions of electrons and holes. Thus the trion composition (i.e., X^+ vs X^-) becomes crucial to the value of the binding energy when the localization diameter changes.

Our numerical method is an extension of the Path Integral approach of Ref. 24. The method does not involve expansions in terms of basis functions, no symmetry assumptions are made (in this sense it can be considered as first principle), and the error can be managed in a controllable way.[25]

The paper is organized as follows. In Sec. II we present and discuss the Hamiltonian for the exciton, biexciton, and charged excitons in a quantum well with interface defects.

We also discuss the approximations used in the present calculations. In Sec. III we introduce the basic ideas of the numerical method, i.e., Path Integral Monte Carlo (PIMC), used to obtain the ground state of the excitonic complexes. In Sec. IV we compare the correlation, localization, and binding energy of the localized exciton (X), biexciton (X_2), and charged excitons ($X^{\pm}$) ground state with the ones of the nonlocalized, i.e., free exciton complexes in a quantum well. Furthermore, we study the dependence of the X, $X^{\pm}$, and X_2 ground state properties on the defect width and height. In Sec. V we compare our calculations with the available experimental data and, finally, present our conclusions in Sec. VI.

II. THE THEORETICAL MODEL

We consider a single GaAs quantum well grown between two Al_xGa_{1-x} As barriers. The effective mass framework is used to describe the semiconductor material and the QW structure. Using the isotropic approximation the Hamiltonian for N_e electrons and N_h holes reads:

$$H = \sum_{i=1}^{N_e,N_h} \left[-\frac{\hbar^2}{2m_i}\nabla^2 + V_{e(h)}(z_i) + V_{e(h)}^{\mathrm{loc}}(\mathbf{r_i}) \right] + \sum_{i<j}^{N_e,N_h} \frac{e_i\, e_j}{\epsilon|\mathbf{r}_i - \mathbf{r}_j|}, \tag{1}$$

where m_i and e_i are the mass and charge of the ith particle, ϵ is the dielectric constant, which we assume equal for the well and for the barrier, $V_{e(h)}$ is the confinement potential associated with the presence of the QW, $V_{e(h)}^{\mathrm{loc}}$ is the lateral (localization) confinement which is due to the fluctuations of the QW width. We take the quantum well growth direction as the z direction.

For a $GaAs/Al_xGa_{1-x}As$ quantum well, we consider the following heights of the square-well potential: $V_e = 0.57 \times (1.155x + 0.37x^2)$ eV for electrons and $V_h = 0.43 \times (1.155x + 0.37x^2)$ eV for holes. In our calculations we use an Al concentration of $x = 0.3$. Furthermore, the following material parameters are used: $\epsilon = 12.58$, $m_e = 0.067\, m_0$, $m_h = 0.34\, m_0$, where m_0 is the mass of the free electron. The units for energy and distance are $H_a^* = 2R_y^* = e^2/(\epsilon\, a_B) = 11.58$ meV, $a_B = \hbar^2\epsilon/(m_e\, e^2) = 99.7$ Å, respectively. We have also considered the case of an anisotropic hole mass according to Ref. 26, using for the in-plane hole mass a smaller value of $m_h^{\parallel} = 0.112 m_0$, and in the quantum well growth direction $m_h^z = 0.377 m_0$. Comparing the binding energies calculated with the isotropic and anisotropic approximations gives important insight about the relevance of band structure details for the properties of excitonic complexes in quantum wells.

The actual shape of the interface defects is not known and depends on the sample growth conditions. To limit the number of parameters, we simulate the interface defects through a cylindrically symmetric potential with a lateral radius R and height $V_{e,h}^{\mathrm{loc}}$. The potential height is determined by the zero-point energy and was obtained as the difference between the lowest energy levels of the electron (hole) in two QWs with the widths L and $L+\delta$, where $\delta = na$ with $n = 1, 2$ and a is the thickness of a single monolayer. Because of the difference in mass between the electron and the hole, the height of the localization potential will also be different (see Fig. 1). For large well widths (L) the localization potential is given by $(\hbar^2\pi^2/m_i)\delta/L^3$. Notice that in Fig. 1 for small L the electron localization has a local maximum which is due to the increased penetration of the electron wave function into the barrier material. For the hole this occurs at much smaller L due to its larger mass.

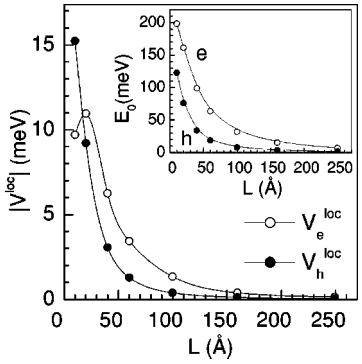

FIG. 1. Dependence of the height of the localization potential $V_{e(h)}^{\mathrm{loc}}$, Eq. (5), for electrons (open dots) and holes (full dots) on the well width L for a well-width fluctuation of 1 ML. Inset: the lowest energy level in the potential, $V_{e(h)}$, vs the well width.

In GaAs, 1 (2) monolayer(s) correspond to a well-width fluctuation of $\delta = 2.8$ (5.6) Å. These parameters ensure that the exciton (trion, biexciton) wave function in the growth direction z is practically not affected by the defect. It is very instructive to see from Fig. 1 that, for narrow QWs, this lateral localization potential reaches about 15 meV which is comparable to the exciton binding energy and is several times larger than the trion binding energy. This behavior is in qualitative and quantitative agreement with the monolayer splitting measured experimentally.[19] In the inset of Fig. 1 we plot the value of the lowest energy level in a QW as a function of the QW width. The main figure can be obtained directly from the results of the inset through $V^{\mathrm{loc}} = E_0(L+\delta) - E_0(L)$.

We proceed further with the assumption that the QW confinement is sufficiently strong and that the Coulomb interaction among the particles in the z direction will not modify the wave functions in the z direction, and consequently we may use in the z direction the noninteracting electron and hole wave functions. In this *adiabatic approximation* we neglect the influence of in-plane electron-hole correlations on their motion perpendicular to the QW plane. This assumption is valid due to the strong quantization in square wells of widths $L \lesssim a_B$, giving rise to the condition on the energies: $\Delta E_{e(h)}^z \gg E_c, E_b^X, E_b^{X_2}, E_b^{X^{\pm}}$, where $\Delta E_{e(h)}^z$ is the level spacing in the quantum well, and E_c, E_b^X, $E_b^{X_2}$, $E_b^{X^{\pm}}$ are the correlation and binding energy of exciton, biexciton, and trions, respectively.

Our approach to compute the binding energies starts from the N-particle ($N = 2, 3$, and 4) density matrix of the excitonic complex of interest (exciton, trion, and biexciton) which is obtained from a solution of the corresponding Bloch equation, see Ref. 24. In the adiabatic approximation, the full N-particle density matrix factorizes into

$$\rho(\mathbf{R}^{xyz},\beta) = \rho(Z_e,\beta)\rho(Z_h,\beta)\rho(\mathbf{R}^{xy},\beta), \tag{2}$$

where $\mathbf{R}^{xyz}(\mathbf{R}^{xy}) = \{\mathbf{r}_{e1},\mathbf{r}_{e2},\ldots,\mathbf{r}_{eN_e};\mathbf{r}_{h1},\mathbf{r}_{h2},\ldots,\mathbf{r}_{hN_h}\}$ is a 3D (2D) vector of all particle coordinates, $Z_{e(h)}$ is the z coordinate of all electrons (holes), $\rho(Z_e,\beta)$ and $\rho(Z_h,\beta)$ are the density matrices of free electrons and holes confined in the z direction by the square well, and $\beta = 1/k_BT$ is the inverse temperature. We underline that the density matrix $\rho(\mathbf{R}^{xy},\beta)$ contains all in-plane electron-hole correlations and fully includes the effect of the localization potential. It obeys the two-dimensional N-particle Bloch equation which is obtained by averaging the three-dimensional Bloch equation over z and using Eq. (1) and the ansatz in Eq. (2):

$$\frac{\partial}{\partial\beta}\rho(\mathbf{R}^{xy},\beta) = \left(-\sum_{i=1}^{N_e,N_h}\frac{\hbar^2}{2m_i}\nabla_{xy}^2 + V_{\text{eff}}^{xy} + V_{e(h)}^{loc,xy}\right)\rho(\mathbf{R}^{xy},\beta). \tag{3}$$

Here, we have introduced an effective 2D in-plane interaction potential V_{eff}^{xy}:

$$V_{\text{eff}}^{xy}(\beta) = \int dZ_e\, dZ_h \sum_{i<j}\frac{e_i\, e_j}{\epsilon|\mathbf{r}_i-\mathbf{r}_j|}\rho(Z_e,\beta)\rho(Z_h,\beta) \times\left[\int dZ_e\, dZ_h\, \rho(Z_e,\beta)\rho(Z_h,\beta)\right]^{-1}. \tag{4}$$

and the total localization potential

$$V_D^{\text{loc},xy} = \begin{cases} E_0(L+\delta) - E_0(L), & \text{if } \sqrt{(x^2+y^2)} \leqslant D/2; \\ 0, & \text{if } \sqrt{(x^2+y^2)} > D/2, \end{cases} \tag{5}$$

where $E_0(L)$ is the lowest energy level in a QW of widths L (see inset of Fig. 1).

III. NUMERICAL SIMULATION APPROACH

We numerically solve the Bloch equation ((3)) using the path integral representation of the density matrix. Using the operator identity $e^{-\beta H} = (e^{-\tau H})^M$, the density matrix at inverse temperature β can be expressed in terms of M density matrices, each taken at a M times higher temperature $M\, k_BT$, or as a path integral with M steps of size $\tau = 1/(Mk_BT)$:[25]

$$\rho(\mathbf{R},\mathbf{R};\beta) = \int d\mathbf{R}_1 \ldots \int d\mathbf{R}_{M-1}\sum_P \frac{(-1)^{\delta P}}{N!} \times\langle\mathbf{R}|e^{-\tau\hat{H}}|\mathbf{R}_1\rangle\ldots\langle\mathbf{R}_{M-1}|e^{-\tau\hat{H}}|\hat{P}\mathbf{R}\rangle, \tag{6}$$

where $\mathbf{R}$ represents a set of coordinates of N particles in two dimensions; $\hat{P}$ is the N-particle exchange operator, $(-1)^{\delta P}$ denotes the sign of the permutation for Fermi particles (electrons and holes); $\rho(\mathbf{R},\mathbf{R}';\tau) = \langle\mathbf{R}|e^{-\tau\hat{H}}|\mathbf{R}'\rangle$ is the coordinate representation of the N-particle density matrix at the new inverse temperature τ. For the N-particle high-temperature density matrix, $\rho(\mathbf{R},\mathbf{R}';\tau)$, we use the pair approximation which is valid for $\tau \leqslant 1/(3\, H_a^*)$:

$$\rho(\mathbf{R},\mathbf{R}';\tau) \approx \prod_i^N \rho^{[1]}(\mathbf{r}_i,\mathbf{r}_i;\tau)\prod_{j<k}\frac{\rho^{[2]}(\mathbf{r}_j,\mathbf{r}_k,\mathbf{r}_j',\mathbf{r}_k';\tau)}{\rho^{[1]}(\mathbf{r}_i,\mathbf{r}_i';\tau)\rho^{[1]}(\mathbf{r}_k,\mathbf{r}_k';\tau)} + O(\rho^{[3]}), \tag{7}$$

where i,j are particle indices and $\rho^{[1]}(\rho^{[2]})$ is the one(two)-particle density matrix. The one-particle density matrix, $\rho^{[1]}$, is the known free-particle kinetic energy density matrix. The pair density matrix $\rho^{[2]}$ was obtained from a direct numerical solution of the two-particle Bloch equation for which we used the matrix squaring technique.[27,28]

As one can see from Eq. (6), the needed diagonal matrix elements of the low-temperature density operator are expressed in terms of all diagonal and off-diagonal matrix elements of the corresponding high-temperature density operator which can be effectively computed using path integral Monte Carlo simulations, see Ref. 24 and references therein. Obviously, for these simulations to be efficient, it is crucial that the off-diagonal density matrix, $\rho^{[2]}$, can be quickly evaluated for any given initial ($\mathbf{r}_i$, $\mathbf{r}_j$) and final ($\mathbf{r}_i'$,$\mathbf{r}_j'$) radius vectors of the particle positions. For this reason, before doing the PIMC simulations, we calculated in advance tables of the pair density matrices (DM) for each type of interaction in our system. In our electron-hole system in a QW with the localization potential, we needed to calculate: (i) three tables of pair density matrices corresponding to electron–electron, hole–hole, and electron-hole interactions given by the two-particle Bloch equation with the smoothened effective 2D Coulomb potential, see Eq. (4), and (ii) two tables with the density matrix of a single particle (electron or hole) in a 2D cylinder of finite height (for particles localized at the interface defect). The contributions of all these interactions (correlations) can be treated as additive, once the used high-temperature pair density matrices correspond to sufficiently high temperature (such that commutators of pairs of energy contributions are negligibly small). Finally, using the pair DM tables, we are able to calculate the many-body density matrix, Eq. (7), for any set of initial $\mathbf{R}$ and final $\mathbf{R}'$ positions of all particles. We substitute this expression into Eq. (6) and perform the high dimensional integration using a multilevel (bisection) Metropolis algorithm (see, e.g., Ref. 28).

In the present calculations we used tables of the pair density matrices at a temperature three times the effective electron-hole Hartree, i.e., $1/\tau = 3H_a^* = 403$ K. By choosing in Eq. (6) the number of factors equal to $M = 270$, the full density matrix, $\rho(\mathbf{R},\mathbf{R};\beta)$ and all thermodynamic quantities can be accurately evaluated at a temperature $T = 1.49$ K. All results shown below correspond to this temperature value.

Before considering in detail the effect of quantum well-width fluctuations on the binding energies of excitonic complexes, we recall the main results obtained for *ideal* QWs with finite width L.[24] Quasi-two-dimensional systems like GaAs QWs have been extensively investigated in the last years, both experimentally[1,2,4–10] and theoretically.[12–16] These studies revealed that, due to the confinement, the 2D excitonic states have binding energies which are several times larger than the binding energies in the bulk materials. This effect is mainly due to the confinement of the carrier wave functions along the structure growth direction, which

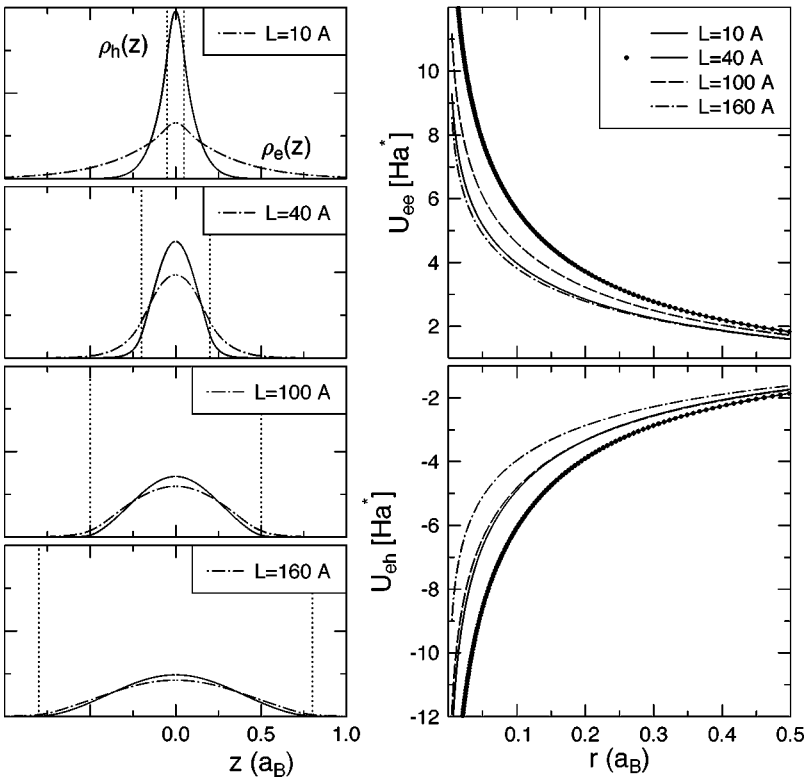

FIG. 2. Left: electron $\rho_e(z)$ and hole $\rho_h(z)$ density matrix in the QW (dotted lines indicate QW walls). Right: QW width dependence of the effective electron–electron (ee) and electron–hole (eh) potentials, see Eq. (4).

leads to a two-dimensional character of excitons and, consequently, to a change in the in-plane interaction potential between the carriers. In the framework of the *adiabatic approximation* these changes can be easily seen in the effective in-plane potential V_{eff}^{xy}, Eq. (4), which depends on the quantum well-width L as a result of the integration in Eq. (4) over the free electron and hole density matrices which reflect the probability distributions of an electron and hole in the square well potential of given width L. In Fig. 2, we present the electron and hole densities in the square well with a width varying between 10 and 160 Å. The results on the left-hand side of Fig. 2 confirm that, due to the smaller mass, the electron is less localized than the hole and, for $L \leqslant 20$ Å, most of the electron density resides in the barrier material.

The effective in-plane potential V_{eff}^{xy} is shown on the right-hand side of Fig. 2. Notice that it depends on L in a nonmonotonic way reaching a maximum (absolute) value around $L \approx 40$ Å. Such an increase with decreasing L (for not too small values of L) is also found experimentally and theoretically and is due to an increase in the interparticle correlations and results in the main contribution to the increase of the binding energies in ideal quantum wells at intermediate QW widths.

IV. BINDING ENERGIES

In this section we investigate the combined influence of the finite QW width and of the interface defects (defect width and height) on the ground state of the exciton and excitonic complexes. In particular, we analyze the modification of the binding energies and of the average interparticle distances in the ground state of excitons (X), positive and negative trions ($X^{\pm}$), and biexcitons (X_2).

A. Binding energies and average size of excitonic complexes

For an ideal QW, i.e., without interface defects, we define the binding energy of the exciton, charged exciton and biexciton as:

$$E_B(X) = E_e + E_h - E(X),$$

$$E_B(X^{\pm}) = E(X) + E_{h(e)} - E(X^{\pm}),$$

$$E_B(X_2) = 2E(X) - E(X_2), \tag{8}$$

where $E_{e(h)}$ is the energy of a single electron (hole) in the given quantum well with a free particle mean kinetic (thermal) energy k_BT, and $E(A)$ is the total energy of the excitonic complex A. If an interface defect is present and a localization potential is included in our calculations, then the above definitions must be modified. All energies must be replaced by the corresponding energies of particles localized in the defect potential. The corresponding generalized expressions will be given in Sec. IV B.

Using a finite temperature approach such as PIMC, one calculates states in thermal equilibrium. Moreover, when the temperature is not sufficiently low and comparable with the depth of the trapping potential, the *equilibrium state* reached in a sufficiently long simulation will correspond to nonlocalized states rather than localized ones. To correctly obtain the total and binding energies of localized excitonic complexes, the results were computed not by averaging over all states, but by restricting the average to the states localized in the trapping potential.

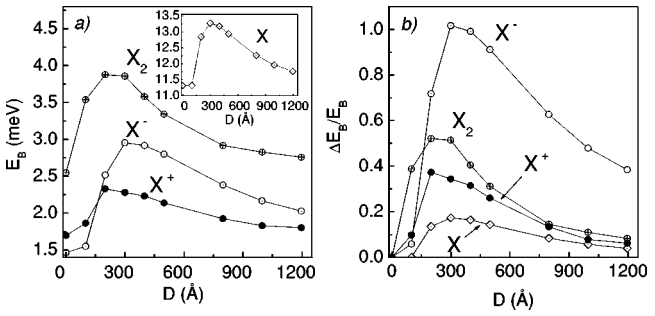

FIG. 3. (a) Binding energies of various excitonic complexes vs the diameter of the 1 ML quantum well width fluctuation for a QW width of $L=60$ Å and temperature, $T=1.5$ K; (b) the same as (a) but now for the relative increase of the binding energy.

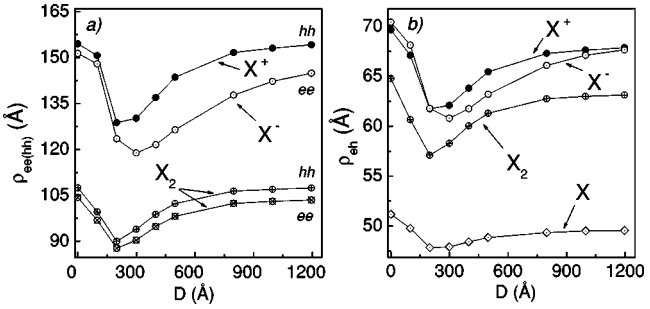

FIG. 4. Average distance between the constituents of the different excitonic complexes as a function of D for (a) equally charged and (b) oppositely charged particles.

We now discuss the results for the binding energies and average interparticle distance in the ground state of various excitonic complexes as a function of the depth and width of the interface defects. In Fig. 3(a) we plot the binding energies versus the diameter of the trapping potential, D, for the case of a 1 monolayer (1 ML) surface defect. The corresponding relative gain in the binding energies due to the interface defect is shown in Fig. 3(b). As an example, we took a QW width of $L=60$ Å and a 1 ML QW width fluctuation which corresponds to the following heights of the electron and hole localization potentials, $|V_e^{\mathrm{loc}}|=3.43$ meV and $|V_h^{\mathrm{loc}}|=1.28$ meV, respectively. From Fig. 3 one can notice that for all excitonic complexes the binding energy is always larger when a defect is present than in the ideal case. In particular, it increases with the diameter D of the trapping potential up to some maximum after which it slowly decreases. However, for very large D the system approaches very slowly the ideal QW result, but 1 ML wider than the original one.

Notice that the position of the maximum is different for the different excitonic complexes. This is readily explained by the different lateral size of different bound states which is determined by the lateral extension of the electron and hole wave functions in the trap and by their relative distance. The electrons are more sensitive to the defect because the trapping potential has a larger effect on their localization (the holes are substantially localized even in the absence of the defect). Furthermore, we observe that the lateral confinement has a very different effect on the magnitude of the exciton, trion, and biexciton binding energies [see Fig. 3(b)]. In particular, the exciton binding energy is only relatively weakly affected by the localization, i.e., a very small peak in the relative binding energy gain of less than 20% occurs. In contrast, the binding energy of the negatively charged exciton increases by more than 100%, from 1.4 to 3 meV for the localization potential of diameter $D\approx 300$ Å.

Figure 4 shows the average in-plane interparticle distance, ρ_{ij}, versus the diameter of the localization trap for the exciton, trions, and biexciton. For a 2D system this results, after using the adiabatic approximation, in the following expression:

$$\rho_{ij}=\int_0^\infty r_{ij}\, g(r_{ij})dr_{ij} \Big/ \int_0^\infty g(r_{ij})dr_{ij}, \tag{9}$$

where $g(r_{ij})$ is the pair distribution function of the particles i and j.

By comparing the electron-hole distances in various complexes, see Fig. 4(b), it can be seen that the electron-hole distance in the exciton, i.e., the size of the exciton, is about 1.2–1.4 times smaller than the electron-hole separation in the charged excitons and about 3 times smaller than the average electron–electron (hole–hole) distances, Fig. 4(a). This explains our previous finding, see Fig. 3(b), that the exciton state is much less influenced by the lateral confinement than the X^-. In the exciton, where the electron and hole are coupled much stronger, the interparticle distance changes only slightly with the diameter D and the effect on their binding energy is weak. Notice also that the peak in the gain of the binding energy quite closely follows the minima of the electron-hole interparticle distances. This result agrees well with the experimental findings (discussed below) that in the case of localized particles the binding energy of the X^- exceeds that of the X^+.

Furthermore, it is interesting to note that the biexciton appears to be *less extended* than the trions, thus explaining the fact that trions have a lower binding energy than the biexciton, see Fig. 3(a). This is consistent with the experimental observations, which will be discussed in detail in Sec. V. At the same time, the biexciton is more affected by the interface defect than the positive trion, see Fig. 3(b). This suggests that the number of electrons in the excitonic complexes plays a much more important role in the interaction with the interface defect than the number of holes. In fact, both the X^- and X_2, which contain two electrons, are more influenced by the localization than the X and X^+. The reason is that the localization potential has a stronger impact on the confinement of electrons than on holes, as noted above.

Next, we compare the negative and the positive trion. For small localization islands, $D\leqslant 150$ Å, the average distances between electrons in X^- and holes in X^+ are very similar and, consequently, the relative gain in the binding energies of the two trions is close as well, see Fig. 3(b). In contrast, for wide localization islands, i.e., $D\geqslant 200$ Å, the behavior of the two trions differs significantly, e.g., the binding energies and the interparticle distances between the respective pair of equally

charged particles deviate from each other, see Figs. 3 and 4. The reason is a different influence of the QW potential on the electron and hole wave functions in the X^- and X^+ states. In a quantum well the electrons are substantially extended into the barrier material (i.e., in the z direction), whereas the holes are much more confined, see Fig. 2(a). This leads to a significantly larger overlap of the two electrons in the X^- state compared to the two holes in the X^+ and to a weaker in-plane effective electron–electron interaction potential, Eq. (4). As a result, in Fig. 4(a) at $D=0$ we can see that the electron–electron distances, ρ_{ee}, are slightly smaller than those of the holes, ρ_{hh}. Though the average distances in the X^- and X^+ states are very similar, if one compares fluctuations of the average distances, $\delta\rho=\sqrt{\langle\rho^2\rangle-\langle\rho\rangle^2}$, they will be much larger for the electrons in the negative trion X^-. This can be seen directly from the behavior of the pair distribution functions [see in Figs. 7(a) and 7(b)]. When the trions are localized by the additional lateral confinement these fluctuations are quenched and the distance between particles of the same charge is decreased, e.g., for $0 \leqslant D \leqslant 300$ Å. This must have a stronger effect on the electrons than on the holes. The stronger repulsive interaction between the holes in the X^+ state reduces to a larger extent the gain in the binding energy as compared to the X^- state, where the electron interaction is weaker and particles can be brought to smaller distances. This accounts for the increase of the X^- binding energy up to, and even beyond, the X^+ binding energy for large D.

B. Origin of the enhanced binding energies

It turns out that the differences in the trion binding energies are not caused solely by their different spatial extensions, see Fig. 4. In fact, the difference between the average interparticle distances in the two trions is not sufficiently large to account for the gain of the binding energy for the X^- and the X^+, see Fig. 3(b). The explanation must be found in the fact that the gain in the binding energy, as a function of the size of the localization island, does not come only from the changes in the Coulomb interaction related to the interparticle distances, but also from changes (and differences) of the electron and hole localization energies, and the kinetic energy of the particles.

In the presence of the localization potential each electron and hole acquires an additional (single particle) potential energy–-the localization energy $E_{\rm loc}^{e(h)}$. This single particle energy can be directly computed by averaging the localization potential over the radial electron (hole) distribution:

$$E_{\rm loc}^{e(h)}(D) = \int dr_{e(h)}\, g^R(r_{e(h)}) V_D^{\rm loc}(r_{e(h)}) \Big/ \int dr_{e(h)}\, g^R(r_{e(h)}). \tag{10}$$

Similarly, each bound excitonic complex is affected by the localization potential where each electron and hole contributes additionally to the total localization energy:

$$E_{\rm loc}(X) = E_{\rm loc}^{e}(X) + E_{\rm loc}^{h}(X), \tag{11}$$

where $E_{\rm loc}^{e(h)}(X)$ for the exciton is computed in an analogous way as was done for the single particles in Eq. (10), but with the appropriate radial electron (hole) distribution inside the localized exciton. Furthermore, Eq. (10) can be straightforwardly generalized to the trions and biexciton cases.

Obviously, the localization energy modifies the total energy of all particles,

$$E(X) = E(X, D=0) \rightarrow E(X,D); \quad E(X^{\pm}) \rightarrow E(X^{\pm},D);$$

$$E(X_2) \rightarrow E(X_2,D), \tag{12}$$

where for all bound states $(X, X^{\pm}, X_2)$ the total energy can now be written as

$$E(D) = E(0) + \delta E_{\rm Coul}(D) + \delta E_{\rm kin}(D) + E_{\rm loc}(D). \tag{13}$$

Here, $\delta E_{\rm Coul}(D)$ and $\delta E_{\rm kin}(D)$ denote, respectively, the change of the Coulomb and kinetic energy due to the presence of the defect of diameter D. From Eqs. (8) and (13) we can now derive the definition of the binding energy of an exciton in the presence of a localization potential:

$$E_B(X,D) = E_B(X,0) + \delta E_{\rm Coul}(X,D) + \delta E_{\rm kin}(X,D) + \delta E_{\rm loc}(X,D), \tag{14}$$

where we define the change of the localization energy due to the excitonic bound state

$$\delta E_{\rm loc}(X,D) = \delta E_{\rm loc}^{e}(X,D) + \delta E_{\rm loc}^{h}(X,D),$$

$$\delta E_{\rm loc}^{e(h)}(X,D) = E_{\rm loc}^{e(h)}(D) - E_{\rm loc}^{e(h)}(X,D) = \int dr_{e(h)} [g^R(r_{e(h)}) - g^R(r_{e(h)},X)] V_D^{\rm loc}. \tag{15}$$

Similarly, the change of the kinetic and interaction energies of an electron-hole pair forming an exciton is given by

$$\delta E_{\rm kin}(X,D) = E_{\rm kin}^{e}(D) + E_{\rm kin}^{h}(D) - E_{\rm kin}(X,D)$$

$$\delta E_{\rm Coul}(X,D) = - E_{\rm Coul}^{eh}(X,D). \tag{16}$$

These expressions can be generalized directly to the case of the trions and biexciton. For example, for the positive trion the change in the Coulomb interaction is expressed as follows:

$$\delta E_{\rm Coul}(X^+,D) = [E_{\rm Coul}^{eh}(X)] - [2E_{\rm Coul}^{eh}(X^+) + E_{\rm Coul}^{hh}(X^+)]. \tag{17}$$

In Eqs. (16) and (17) the Coulomb energy, $E_{\rm Coul}(D)$, is estimated as an average of the effective potential, $V_{\rm eff}^{xy}$ (Fig. 2), over the pair distribution functions calculated for each type of interparticle interaction. For example, for the electron–hole interaction in the exciton we have:

$$E_{\rm Coul}^{eh}(X) = \int dr\, V_{eh}^{xy}(r) g_{eh}(r,X). \tag{18}$$

The kinetic energy of the localized single electron (hole), $E_{\rm kin}^{e(h)}$, the localized exciton, $E_{\rm kin}(X)$, the trion, $E_{\rm kin}(X^+)$, and the biexciton, $E_{\rm kin}(X_2)$, were computed as the difference between the total energy and the full potential energy which includes both Coulomb interaction and localization energy,

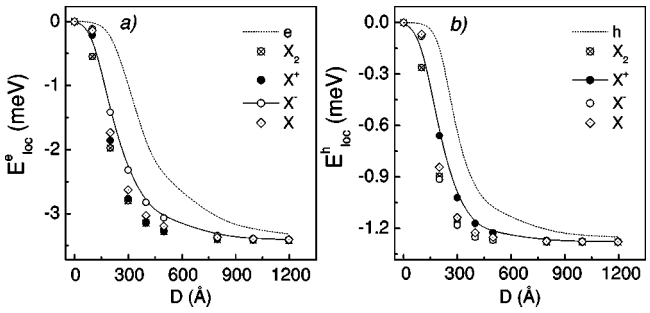

FIG. 5. Localization energy of an electron (a) and hole (b) in the different excitonic complexes as a function of diameter of the localization island for a one monolayer fluctuation and QW width of $L=60$ Å. Dotted lines are the corresponding localization energies of a single electron and hole in the same localization potential.

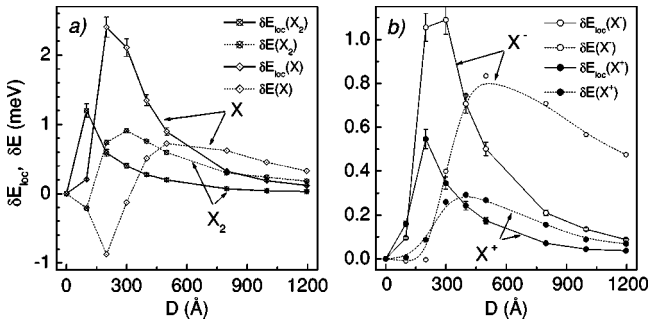

FIG. 6. (a) Localization energy gain, δE_{loc} [Eq. (15)], and energy gain, δE, of the exciton and biexciton vs diameter of the localization island. (b) Comparison of the same energies for positive and negative trions. The same parameters are used as in Fig. 5.

$E_{\mathrm{kin}}=E-(E_{\mathrm{Coul}}+E_{\mathrm{loc}})$. This result can be compared with a more strict thermodynamic estimator of the kinetic energy as the mass derivative of the partition function, $E_{\mathrm{kin}}=(m/\beta Z)\times(\partial Z/\partial m)$. We found that both expressions give very similar results.

In Fig. 5 we show the contribution of the well-width fluctuation, which we will call the localization energies, to the single (noninteracting) particles, $E_{\mathrm{loc}}^{e(h)}$, and interacting electrons (holes) in various excitonic complexes: $E_{\mathrm{loc}}^{e(h)}(X)$, $E_{\mathrm{loc}}^{e(h)}(X^{\pm})$, and $E_{\mathrm{loc}}^{e(h)}(X_2)$. This energy was estimated as an average of the localization potential, $V_D^{\mathrm{loc},xy}$ [Eq. (5)], over the radial distribution functions calculated separately for electrons and holes, see, e.g., Figs. 7(c) and 7(d). For large D, $E_{\mathrm{loc}}^{e(h)}$ should approach the depth of the in-plane localization potential, i.e., $|V_e^{\mathrm{loc}}|=3.43$ meV and $|V_h^{\mathrm{loc}}|=1.28$ meV. As one can see, the interparticle interaction significantly increases the localization. Both in the left and right insets of Fig. 5, the localization energy of a single particle (electron or hole) shown by the dotted line is much less (in absolute value) compared to that of the $X, X^{\pm}, X_2$ and saturates only for $D \geqslant 1200$ Å. The explanation is that the attraction between electrons and holes already leads to significant spatial localization of the particles compared to the free particle thermal wavelength and, as a consequence, the effective localization potential felt by each particle (the potential is smoothened over the particle's wave functions) is deeper.

An interesting point that we notice in Fig. 5 is that, on average, the electrons and holes in the biexciton are more localized than in all other bound states. The only exception is the localization energy of the hole in the range 200 Å$\leqslant D \leqslant$300 Å when a single hole in the X^- state tends to be more localized, see Fig. 5(b). Among all considered bound states only the biexciton appears to be strongly localized for islands with a diameter around $D\approx 100$ Å (other excitonic states, in our simulations at temperature $T\approx 1.5$ K, have a much higher probability to become delocalized due to thermal fluctuations). This is confirmed by the gain in the binding energy shown in Fig. 3(b), where at the point $D\approx 100$ Å only the biexciton shows a strong increase by 40%, and in Fig. 5 at $D=100$ Å only the biexciton shows non-negligible values for the localization energy, $E_{\mathrm{loc}}^{e}=0.54$ meV and $E_{\mathrm{loc}}^{h}=0.25$ meV, for the electron and the hole, respectively.

Now, using the values of the localization energies of the electrons and the holes shown in Fig. 5, one can estimate the total localization energies of the different excitonic complexes, e.g., the localization energies of the negative trion and the biexciton can be estimated as follows:

$$E_{\mathrm{loc}}(X^-) = 2E_{\mathrm{loc}}^{e}(X^-) + E_{\mathrm{loc}}^{h}(X^-),$$

$$E_{\mathrm{loc}}(X_2) = 2E_{\mathrm{loc}}^{e}(X_2) + 2E_{\mathrm{loc}}^{h}(X_2). \tag{19}$$

These energies include many-body correlation effects in combination with the specific radial distribution functions which are different for each bound state, see e.g., Figs. 7(c) and 7(d).

We now analyze the binding energies which are modified from their ideal expression, Eq. (8), due to the three localization corrections, cf. Eqs. (14) and (15), namely the contributions due to changes of the Coulomb interaction, kinetic, and localization energy. Each part can be calculated separately and the results are presented in Figs. 6(a) and 6(b). Solid lines in this figure show changes of the localization energy, $\delta E_{\mathrm{loc}}(D)$, of the exction, trions, and biexciton as a function of the diameter of the island, D. Dotted lines show combined changes in the Coulomb interaction and kinetic energy minus the binding energy in the same QW without the interface defect, $\delta E(D)=\delta E_{\mathrm{Coul}}(D)+\delta E_{\mathrm{kin}}(D)-E_B(0)$. Consequently,

$$E_B(D) = E_B(0) + \delta E_{\mathrm{loc}}(D) + \delta E(D). \tag{20}$$

In Fig. 6(a) we note that the difference in the localization energies, shown by the solid curves in Figs. 6(a) and 6(b), is maximal for the exciton. This is easy to understand because for the exciton [see Eq. (15)] we subtract from the energies of the unbound electron and hole (which are less localized) the localization energy of a more localized bound electron-hole pair in the exciton state (see Fig. 5). According to Eq. (20) this gives positive contributions to the binding energy, e.g., at the point $D=300$ Å it is about 2 meV. For the biexciton and the negative trion the difference of localization energies reaches a maximum value of about 1 meV. For the biexciton the maximum is reached around the defect diameter $D\approx 100$ Å, for X^- around $D\approx 300$ Å, and for X^+ at $D\approx 200$ Å.

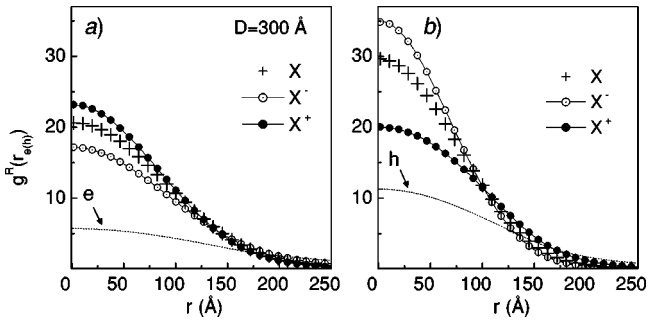

FIG. 7. (a), (b) Radial distribution function of electrons (a) and holes (b) for exciton, positive and negative trions, and the single electron (hole) as a function of distance, $r_{e(h)}$, from the center of the localization potential. The same parameters are used as in Fig. 5.

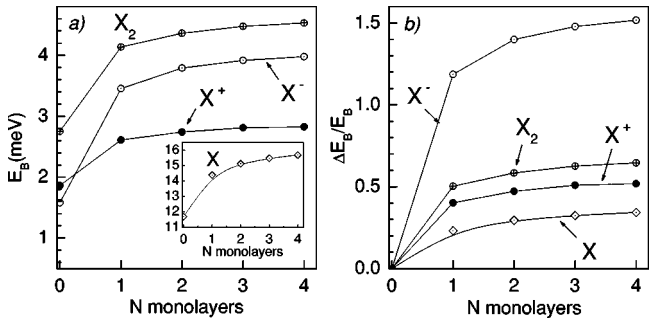

FIG. 8. The same as Fig. 3, but now as a function of the number of monolayers, N, for a fixed QW width of $L=40$ Å, temperature $T=1.5$ K and diameter of the localization potential, $D=400$ Å.

The dotted lines in Figs. 6(a) and 6(b) are the contributions due to the defect induced changes of the Coulomb interaction and kinetic energy. In this way the total binding energy (20) is the sum of the respective solid and dotted curves in Fig. 6. By comparing each pair of curves for X, $X^{\pm}$, and X_2, one can note a general feature valid for all bound states: at $D \leqslant 300$ Å the main contribution to the binding energy comes from changes of the localization energy, Eq. (15), but when the defect diameter exceeds $D \approx 600$ Å the main effect is due to changes of the kinetic energy and the interparticle interaction.

It is interesting that for the exciton and biexciton the quantity ΔE becomes negative in the range of defect diameters $D \leqslant 300$ Å which leads to a reduction of the binding energy. The reason is that δE is composed of δE_{kin} which is negative and the positive term δE_{Coul}. δE_{kin} is negative because the kinetic energies of bound particles are larger than those of unbound particles. This is readily understood because the wave functions of bound particles are more localized (spatially less extended) and thus have a larger curvature, which increases the kinetic energy. It follows also from the virial theorem that the increase of potential (or interaction) energy leads to an increase of the kinetic energy.

The comparison of δE_{loc} and δE between the positive and negative trions in Fig. 6(b) shows that the negative trion is more affected by the localization for $D \geqslant 100$ Å . This has a direct relation with Fig. 3, where the X^- binding energy exceeds that of the X^+ for all $D \geqslant 150$ Å.

The positive trion X^+ is a much heavier composite particle with two holes and one electron compared to the X^-, where there are two electrons and one hole. As a consequence the X^+ is less mobile and, thus, is less affected by the lateral confinement. This fact can be demonstrated by Figs. 7(a) and 7(b) where we show the radial distribution functions $g^R(r_{e(h)})$ of an exciton, negative/positive trions, and a single electron/hole in a QW of width $L=60$ Å for a defect diameter $D=300$ Å; (a) and (b) show the radial density of electrons and holes, respectively. Notice that at the center of the localization confinement ($r_{e(h)}=0$) the radial density of electrons in the X^- state is increased by more than a factor of 3 as compared to the radial density of a single electron in the same localization potential (curve indicated by "e"). At the same time, comparison of the densities for the holes in the X^+ state and the density of the single hole shows only an increase by a factor of 1.8. These results are in agreement with our previous statement that the localization has a larger effect on electrons than on holes and, consequently, on the composite particles with a larger number of electrons (in our case X^- and X_2). Figures 7(a) and 7(b) also show that the central radial density of electrons is highest in the X^+ state, whereas the highest central radial density of holes is observed in the X^-. In both (a) and (b) the electron and hole radial densities near the localization potential center for the exciton state lies between the corresponding values for the X^+ and X^-. This fact is easily understood from the symmetry of the spatial configuration of particles in the X, X^+, and X^- states in the cylindrical defect potential. For trions, the single hole in the X^- (the single electron in the X^+) will most probably occupy the central position between the two electrons (two holes) to minimize the correlation energy and thus the total energy.

C. Dependence on the number of monolayer fluctuations

Now, we allow for well-width fluctuations larger than 1 ML and analyze the dependence of the binding energies and interparticle distances on the number of monolayers. We fix the quantum well width to $L=40$ Å and the diameter of the defect to $D=400$ Å. In Fig. 8 we plot the binding energy of the different excitonic complexes as a function of the number of monolayers N forming the defect (the curves are guides to the eye since N is a discrete index). Notice that increasing N leads to a monotonic increase in the binding energy for all exciton complexes which saturates for $N \approx 4$. Notice that the increase of the binding energy of the biexciton and of the negative trion is almost parallel. This is a clear confirmation of our earlier conclusion that the lateral confinement of the electron by the defect has a more pronounced effect on the binding energy than the hole confinement. Again we observe that the binding energy of the X^- exceeds that of the X^+ in the presence of a localization potential (see the discussion of Fig. 3). Figure 8 shows that this trend persists in the case of increasing defect depth.

Figure 9 displays the dependence of the mean e–e, h–h, and e–h distances in the different excitonic states on the number of monolayers. All distances (i.e., the spatial extension of all bound states) decrease monotonically with N and saturate around $N=4$.

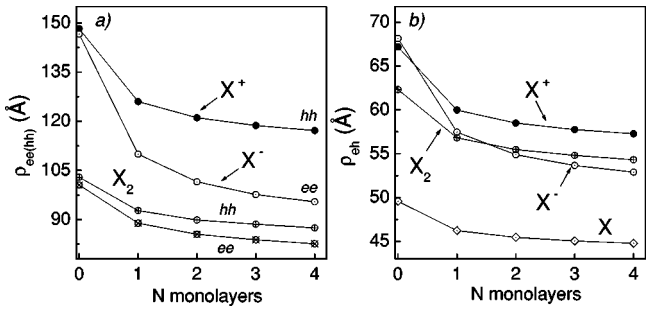

FIG. 9. The same as Fig. 4, but now as a function of the number of monolayers, *N*. Same parameters are used as in Fig. 8.

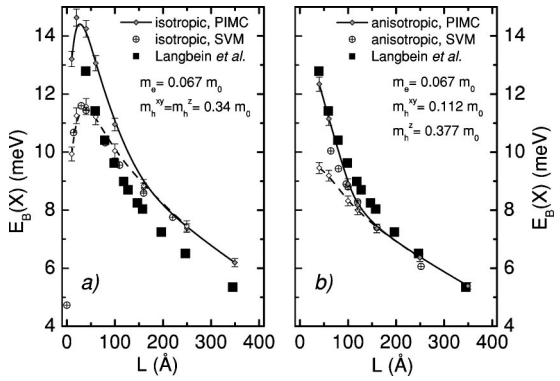

FIG. 10. Exciton binding energies for isotropic (a) and anisotropic (b) hole mass vs quantum well width. Solid square symbols are experimental data of Ref. 10 and circular symbols with a plus sign are obtained from the stochastic variational calculations (Refs. 13 and 14). Full (dashed) lines with small symbols are PIMC results when the localization is included (not included).

V. COMPARISON WITH EXPERIMENT

Before making a comparison between our theoretical results and the experimental data it is necessary to point out a problem that may arise in such a comparison. In particular, one has to be aware of the fact that for finite temperatures there exists an experimental uncertainty about the state in which particles remain after recombination. Namely, particles produced after recombination will typically have a finite kinetic energy which may allow them to leave the localization potential. In this case, the energy of the emitted photon will be reduced by an amount needed to overcome the height of the localization potential. As a consequence, the photoluminescence lines of the exciton complexes exhibit an additional broadening due to the finite kinetic energy of the remaining particles, thus making the determination of the binding energy more complicated.

Second, in experiments there may be two types of measurements of excitons and trions: one, when the excitonic complexes are probed in a single well. These measurements may favor observation of the most strongly localized excitons and trions (as it was found in Ref. 29), while measurements from a QW ensemble favor higher-lying states nearer to the continuum. In the latter case the localization effects do not strongly influence the observed ensemble QW spectra. As the theory shows, this would affect the binding energy, as the localization effects are of great importance in narrow QWs.

A. Exciton binding energy

In Figs. 10(a) and 10(b) we compare the theoretical and experimental binding energies of the exciton as a function of the QW width. Solid and dashed curves in these figures show the binding energy in the QW with defect and in the ideal QW without interface roughness, respectively. The localization potential is considered as due to a well width fluctuation of one monolayer over a circular area of diameter $D=400$ Å in accordance with the experimental findings of Ref. 19. As we can see from Fig. 3 for the QW width around 60 Å this gives an upper bound to the localization effect on the binding energies. In order to be consistent we used the same localization potential when calculating the binding energies of trions and the biexciton.

When using the isotropic approximation for the hole mass ($m_e=0.067m_0$, $m_h^{xy}=m_h^z=0.34m_0$), we notice in Fig. 10(a) that the theoretical results systematically overestimate the binding energy. For example, for $L\geqslant 100$ Å the theory gives binding energies which are $\sim$10% larger than the experimental results. In order to see the effect of the anisotropy of the hole band we performed the calculation using an anisotropic hole mass ($m_h^{xy}=0.112m_0$ in the QW plane and $m_h^z=0.377m_0$ in the QW growth direction[26]) which brings the theoretical points significantly closer to the experiment, see Fig. 10(b). For the QW widths $L\leqslant 100$ Å good agreement is found when the localization effects are included in our model. For example, in Ref. 3 for a QW width $L=34$ Å a value 12.4 meV has been measured for a localized exciton. This agrees quite well with our theoretical prediction of about 12.3 meV for a comparable QW structure ($L=40$ Å).

However, there is still a slight discrepancy between theory and experiment for QW widths in the range $100\leqslant L\leqslant 200$ Å. In this range, in our theoretical model, the localization effects are negligible for excitons. For $L\geqslant 150$ Å the two curves calculated with and without localization practically coincide. In this case, for the wide QWs ($L\geqslant 150$ Å) the theory appears to agree quite well with the experimental binding energies. This allows us to conclude that for such quantum well structures the localization does not play a significant role for excitons and they are not trapped by the interface defects.

In Figs. 10(a) and 10(b) we compare our results with those obtained with the stochastic variational approach,[13,14] both for the isotropic and anisotropic hole masses which gives additional credit to the accuracy of our numerical approach. Note that the hole mass and the dielectric constant used in Refs. 13 and 14 ($m_e=0.067\,m_0$, $m_h^{xy}=0.099\,m_0$, and $\epsilon=12.1$) were slightly different from ours. This leads to minor discrepancies for the binding energies for QW widths smaller than 100 Å because the electron and hole densities in the growth direction are very sensitive to the QW confinement and to the chosen values of electron/ hole masses in narrow QWs (see Fig. 2).

The PIMC results (for the anisotropic hole mass and the 1 ML interface defect of diameter $D=400$ Å) can be com-

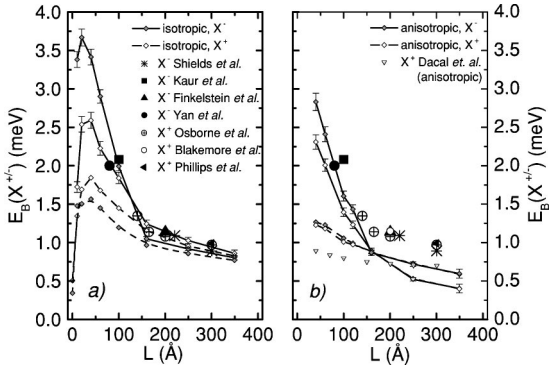

FIG. 11. Trion binding energies for isotropic (a) and anisotropic (b) hole mass vs quantum well width. Symbols are experimental data of Refs. 1 and 2 and theoretical calculations of Ref. 22. Full (dashed) lines with symbols are PIMC results when localization is included (not included).

pared with those of Refs. 20 and 21, where the *exciton binding energy to the interface defect*, $E^D(X)$ has been calculated. This quantity is defined as the difference of the total exciton energy with and without the defect potential. In particular, the variational calculations of Ref. 21 for two types of exciton trial wave functions give, for a QW of width $L=35$ Å and $D=400$ Å, $E^D(X)=7.4$ and 10.4 meV, respectively (the isotropic electron mass is $m_e^z=m_e^{xy}=0.0782m_0$, the heavy hole masses are the same as in the present work). The PIMC calculations for the QW width $L=40$ Å give a similar value, $E^D(X)=8.16$ meV. In the variational calculations of Ref. 20 a value $E^D(X)=3.4$ meV has been reported for a QW with $L=70$ Å. The present calculations give $E^D(X)=3.72$ meV and $E^D(X)=0.84$ meV, for a QW width $L=60$ Å and $L=100$ Å, respectively. This trend definitely shows that the excitons become less localized with increasing QW width.

In conclusion, the comparison of Figs. 10(a) and 10(b) shows that taking into account the anisotropy of the hole mass leads to a decrease of the exciton binding energy compared to the isotropic case. For example, in a 50 Å wide QW this amounts to about 2 meV, and in a 250 Å wide QW it is about 1 meV.

B. Binding energy of positive and negative trions

In Figs. 11(a) and 11(b) we present our results for the binding energy of the trions. We compare our theoretical results with the available experimental data for negative[1] and positive[2] trions, and variational calculations of Ref. 22. First, we can note that the agreement with the experiments is quite good for QW widths $L\geqslant 150$ Å. Specifically, the experimental points for the X^+ are close to our theoretical result, see Fig. 11(a). Unfortunately, for narrow QWs ($L\leqslant 150$ Å) when localization effects become important, there are currently no available experimental data. This would be of high interest as the two points for the X^- reported by Kaur *et al.* and Yan *et al.*[1] show a more rapid increase of the binding energy with the QW width than the one predicted by theory when the localization is not taken into account. On the contrary, calculations with the QW width fluctuations included agree well with these data.

Furthermore, in Fig. 11(a) we observe a crossing of the two binding energy curves (X^+ and X^-) with the localization included near the point $L=135$ Å, and for narrow wells the binding energy of the negative trion becomes larger. For example, in a 40 Å quantum well $E_B(X^-)\approx 3.4$ meV while for the positive trion $E_B(X^+)\approx 2.6$ meV. Preliminary experimental investigations of the X^- and X^+ in the presence of localization[29] seem to confirm these findings and give for a 50 Å wide QW $E_B(X^-)=3.27$ meV and $E_B(X^+)=2.35$ meV. It is interesting to notice that in an ideal QW the situation is the opposite and the binding energy of the X^+ is always larger than that of the X^-. As was already discussed in Sec. IV B the reason is that the localization has a stronger influence on the electrons and, consequently, on the negative trion.

When the anisotropy of the hole mass is included in our calculations we found that there is no crossing between the binding energy of the X^+ and the X^-. A comparison with the variational calculations of Dacal *et al.*[22] [see Fig. 11(b)] also done with the anisotropic hole mass, but slightly different parameters $V_e(V_h)=224.5$ meV (149.6 meV) and $\epsilon=13.2$ [compared to ours $V_e(V_h)=216$ meV (163 meV) and $\epsilon=12.58$], shows some discrepancy with the present calculations for X^+ binding energy in the narrow QWs. This can be due to the following reason. Variational calculations strongly depend on a form of used trial wave functions. In particular, Eq. (3) in Ref. 22 becomes less accurate in the narrow quantum wells and hence requires a larger set of variational parameters. This could lead to a better agreement with the PIMC results.

In Ref. 23 the effect of localization (at the interface defect with a cylindrical symmetry and a Gaussian shape) on the trion binding energy was considered for the anisotropic hole mass with the same parameters as in Ref. 22. It was found that, with the defect present, the X^- binding energy is increased from 0.4 to 0.6 meV in the 150 Å wide QW. However, these values are much lower than the PIMC results which show an increase from 0.90 to 1.02 meV. The results of Ref. 23 are even lower than the value $E_B(X^-)=0.75$ meV reported in Ref. 22 for the same QW width but without the localization effect included. In Ref. 23 the number of basic variational trial wave functions was reduced compared to Ref. 22 and, as the above comparison shows, this appears to be not sufficient for a quantitative description of the trion.

Other theoretical calculations done with an isotropic hole mass and in the absence of a localization potential shown in Fig. 11(a) agree quite well with our data for the ideal QW case. For example, both in Refs. 16 and 30 it was found that the X^+ binding energy is larger by about 20% than the X^- binding energy. This is in agreement with most experimental results which show that the X^+ has a binding energy which is larger than or close to the one of the X^-. However, the theoretical results of Ref. 17 for a 300 Å wide QW showed that $E_B(X^+)$ is lower than $E_B(X^-)$ which is opposite the results of Refs. 16 and 30, but the latter is in agreement with our results for the case of the anisotropic hole mass [see Fig. 11(b)]. From the other hand, the anisotropic calculations show an unsatisfactory agreement between theory and ex-

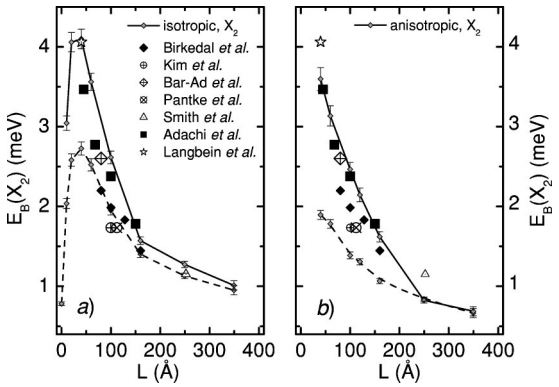

FIG. 12. The same as in Fig. 11 but now for the biexciton binding energy. Symbols are experimental data of Refs. 4–10.

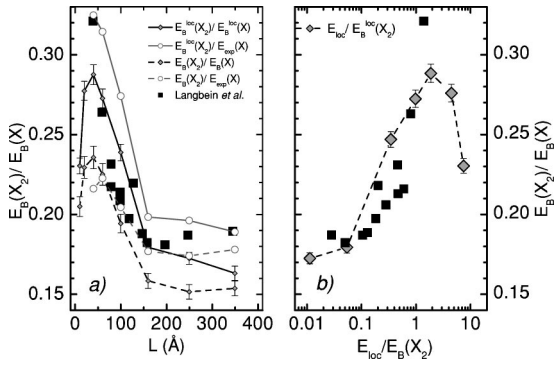

FIG. 13. The biexciton to exciton binding energy ratio (Haynes factor), (a) vs QW width and (b) vs normalized localization potential. Symbols: experimental data for $GaAs/Al_{0.3}Ga_{0.7}As$ QWs (Ref. 10). Curves with symbols: PIMC results. Solid (dashed) curve is the exciton binding energy with (without) localization included; (b) $E_B(X_2)/E_B(X)$ vs localization strength $E_{\rm loc}/E_B(X_2)$. Squares are the experimental data; Rhombii are PIMC results.

periment, in particular for $L>150$ Å where theoretical curves are about 0.5 meV below the experimental points. Here, the localization effects (in the framework of our model) are not important and cannot be the reason for this disagreement.

C. Binding energy of biexciton and the Haynes factor

Now we consider the biexciton binding energy. Solid (dashed) curves in Figs. 12(a) and 12(b) show our theoretical results in the presence (without) of well-width fluctuations which we compare with available experiments[4–10] (symbols in figure). In the case of an isotropic hole mass, we found that with localization taken into account [full line in Fig. 12(a)] the theoretical curve passes through the data of Refs. 5 and 7, but the experimental data of Refs. 4, 6, 8, and 9 agree with the theory for an ideal QW [see the dashed curve in Fig. 12(a)]. The inclusion of the localization effects brings the theoretical curve slightly above the experiment, predicting that in, e.g., a narrow 40 Å wide QW the binding energy of the biexciton is about (4.0–4.1) meV. It is interesting that almost the same experimental result is reported in Ref. 10, where the value 4.1 meV is found for the 40 Å QW. It should be stressed however, that our results for the binding energy, in the presence of a one monolayer well-width fluctuation, are close to an upper limit, since the used defect diameter ($D=400$ Å) was such that it gave practically the maximal gain in the biexciton binding energy as due to localization (see Fig. 3). But this value of the defect diameter, $D=400$ Å was found to be a very good estimate of the characteristic defect size in GaAs quantum wells.[19]

The use of an anisotropic hole mass [see Fig. 12(b)] leads to a reduction of the biexciton binding energy by almost (0.4–0.8) meV. As in the case of trions, for wide QWs with $L\geqslant 150$ Å the anisotropic approximation gives a less satisfactory agreement with the experimental points. From the other hand, for the QW widths $L\geqslant 150$ Å we found excellent agreement with the experiment of Ref. 10 when localization is included in our calculations [see Fig. 12(b), solid curve].

For an anisotropic hole mass and a defect depth of 1 ML, we can compare our results with the variational calculations of Ref. 21. In these calculations, however, a repulsion between particles of the same charge was not taken into account, which makes the comparison only qualitative. In Ref. 21 the biexciton binding energy of about 1.6 and 1.3 meV has been reported for the 30 and 50 Å wide QWs, respectively, and a defect diameter 200 Å. These values of the binding energies are less than our result, 1.9 meV, for a nonlocalized biexciton in a 50 Å wide QW. With the interface defect ($D=400$ Å), the PIMC calculations show an increase of the binding energy up to 3.6 meV, which is close to the experimental data. For example, in Ref. 3, a value $E_B(X_2)=4.2$ meV was attributed to a localized biexciton in a 34 Å wide QW.

In conclusion, the present comparison of the theory and the experiment allows us to conclude that the anisotropic approximation for the hole mass gives better agreement for narrow QWs (with $L<150$ Å). On the other hand, for wide QWs ($L>150$ Å) our model calculations show that the use of isotropic approximation shows better agreement. We expect that the accuracy of the calculations (and of the anisotropic approximation, in particular) can be further improved by taking into account the mismatch of dielectric constants and particle masses in the well and barrier materials. This should lead to a better agreement with the experiment.

In comparing the theory and the experiment, one should keep in mind that different experimental, results have been obtained from different quantum wells which have not been grown under the same conditions and, consequently, their well-width fluctuations may also be different. Nevertheless, overall, the present calculations show that even a simple model of localization can satisfactorily explain the experimental data on the binding energies. We expect that our theory can make reliable predictions if detailed information on the quantum well fluctuations in the samples would be available.

Next, we consider the so-called Haynes factor, which is the ratio between the biexciton and the exciton binding energies, $\nu=E_B(X_2)/E_B(X)$. We compare our results, see Fig. 13(a), with the experimental data of Ref. 10 (solid squares), where the influence of localization on the binding energies of the exciton and biexciton was considered. Here, all theoreti-

cal curves are given only for the isotropic hole mass ($m_h^{xy} = m_h^z = 0.34$) and, as in previous figures, the solid (dashed) line is for the case (without) localization included. The ratio of the exciton and biexciton energies calculated using an anisotropic hole mass is very similar and is therefore not shown.

The lines with small filled symbols are obtained by using the theoretical values of the exciton and biexciton binding energies [Figs. 10(a) and 12(a)], which are denoted as $E_B^{\mathrm{loc}}(X_2)/E_B^{\mathrm{loc}}(X)$ and $E_B(X_2)/E_B(X)$. In addition, since there is a discrepancy between the experimental and the theoretical results in Fig. 10(a) for the exciton binding energy which affects the Haynes factor, we also calculate the Haynes factor as the ratio of the theoretical biexciton binding energy to the exciton energy from the experiment[10] [shown in Fig. 10(a) by the solid squares]. The corresponding results are denoted in Fig. 13(a) as $E_B^{\mathrm{loc}}(X_2)/E_{\mathrm{exp}}(X)$ and $E_B(X_2)/E_{\mathrm{exp}}(X)$.

First, we note that the Haynes factor is practically independent of the QW width for $L \geqslant 150$ Å in agreement with the experiment. However, the value of the constant is different in various cases. When localization is included (solid line) our calculations show a systematic increase of the Haynes factor $\nu = E_B(X_2)/E_B(X)$ by up to 17%. For the exciton and biexciton localized on the interface defect the Haynes factor is $\nu \approx 0.175$, while for the ideal QW, $\nu \approx 0.15$. For well widths $L \geqslant 50$ Å, all theoretical and experimental results exhibit a monotonic decrease of the Haynes factor with increasing L. One can observe that the experimental results are located mainly between the two theoretical curves corresponding to the localized and not localized biexciton. Most of the points lie on the dashed curve with the open circles, $E_B(X_2)/E_{\mathrm{exp}}(X)$, suggesting that the experimentally measured binding energies correspond to nonlocalized biexcitons, but some of the data are substantially above the dashed curve and agree better with the assumption of predominantly localized biexcitons. This is the case for well width $L \leqslant 80$ Å where a strong increase of the Haynes factor is also found from the theory. For example, our theory gives a maximum value $\nu = 0.24$ without localization and $\nu = 0.29$ for localized particles.

Notice that the agreement between the experimental and theoretical results with localization is also confirmed by Fig. 13(b), where the Haynes factor is plotted against the normalized localization potential. We compute the localization energy E_{loc} as the difference between the energy of the localized and nonlocalized excitonic complex (in Ref. 10 the localization energy was defined from the full width at half maximum of the heavy-hole exciton absorption line). As follows from our theory, below 150 Å well thickness when the localization energy becomes of the order of the biexciton binding energy an enhancement of the Haynes factor is observed. This indicates that localization has a crucial effect on the Haynes factor and it must be taken into account for a correct interpretation of the experimental results.

VI. CONCLUSION

In summary, using a path integral Monte Carlo approach, we made a detailed analysis of different excitonic complexes in GaAs/AlGaAs quantum wells. We calculated and analyzed the exciton, trion, and biexciton binding energies, pair distribution functions and mean interparticle distances in the excitonic complexes in a wide range of QW widths. Our method is based on first principles and does not invoke expansions in eigenfunctions. The approach is general, flexible and, what is also important, is not limited to certain specific symmetries of the particle wave function. It allows for a simultaneous account of QW confinement, localization, and valence band anisotropy, and thus can give an accurate theoretical treatment of many experimental systems. The only assumption {the adiabatic approximation [Eq. (2)]} appears to be justified for the present application. Simple estimates show that its accuracy may be reduced for wide QWs with $L \geqslant 250$ Å.

Extending our previous analysis,[24] we concentrated on the influence of disorder, i.e., of the effect of QW width fluctuations on the binding energies. The observed increase of the binding energies in the presence of disorder is in good quantitative agreement with the available experimental data. Furthermore, we analyzed the influence of valence band anisotropy (hole mass) and found that, in some cases (in particular for the exciton and biexciton binding energy) this effect is important in order to achieve agreement with the experimental data.

We also analyzed the case of deep interface defects corresponding to several monolayers depth and found that this can give an additional 20%–30% increase of the binding energy compared to the single monolayer case. This increase is even more pronounced for the negative trion and the biexciton.

The present analysis is the first one in which exciton, trions and biexciton are treated on an equal footing and in which the same size and shape of the QW width fluctuation is invoked for different QW widths. We assumed a 1ML QW width fluctuation over a circular area of diameter $D = 400$ Å. No other fitting parameters were introduced. This led to an overall good agreement of the well-width dependence of the exciton, trions, and biexciton binding energies. It is expected that a better fit with experiment is possible if, e.g., we allow for a noncircular shape of the well-width fluctuation where the anisotropic localization potential will be related to specific crystallographic directions.

Our results have two important implications which can be useful in the interpretation of experimental data. First, comparing the measured binding energy with our numerical calculations for different defect sizes allows one to characterize certain experimental parameters, such as the magnitude of the disorder in a given sample. Second, one can verify or predict whether or not the observed excitonic states are localized or delocalized in a given experimental setup.

ACKNOWLEDGMENTS

The authors would like to thank A. S. Bracker and D. Gammon for making available their experimental results prior to publication. This work was supported by the Flemish Science Foundation (FWO-Vl), the Belgian Interuniversity Attraction Poles (IUAP), the European Commission

GROWTH Programme NANOMAT Project, Contract No. G5RD-CT-2001-00545 and by grants for CPU time at the Rostock Linux-Cluster "Fermion." A. Filinov gratefully acknowledges the hospitality of the Physics Department of the University of Antwerp. Clara Riva is a FWO-Vl Postdoctoral Fellow.

[1] R. Kaur, A. J. Shields, J. L. Osborne, M. Y. Simmons, D. A. Ritchie, and M. Pepper, Phys. Status Solidi A **178**, 465 (2000); G. Finkelstein, H. Shtrikman, and I. Bar-Joseph, Phys. Rev. B **53**, R1709 (1996); A. J. Shields, M. Pepper, D. A. Ritchie, M. Y. Simmons, and G. A. C. Jones, *ibid.* **51**, 18049 (1995); Z. C. Yan, E. Goovaerts, C. Van Hoof, A. Bouwen, and G. Borghs, *ibid.* **52**, 5907 (1995).

[2] J. L. Osborne, A. J. Shields, M. Pepper, F. M. Bolton, and D. A. Ritchie, Phys. Rev. B **53**, 13002 (1996); J. S. Blakemore, J. Appl. Phys. **53**, R123 (1982); J. C. Phillips, *Bonds and Bands in Semiconductors* (Academic, London, 1973).

[3] K. Brunner, G. Abstreiter, G. Böhm, G. Tränkle, and G. Weimann, Phys. Rev. Lett. **73**, 1138 (1994).

[4] D. Birkedal, J. Singh, V. G. Lyssenko, J. Erland, and J. M. Hvam, Phys. Rev. Lett. **76**, 672 (1996).

[5] S. Adachi, T. Miyashita, S. Takeyama, Y. Takagi, A. Tackeuchi, and M. Nakayama, Phys. Rev. B **55**, 1654 (1997).

[6] K. H. Pantke, D. Oberhauser, V. G. Lyssenko, J. M. Hvam, and G. Weimann, Phys. Rev. B **47**, 2413 (1993).

[7] S. Bar-Ad and I. Bar-Joseph, Phys. Rev. Lett. **68**, 349 (1992).

[8] J. Kim, D. Wake, and J. Wolfe, Phys. Rev. B **50**, 15099 (1994).

[9] G. Smith, E. Mayer, J. Kuhl, and K. Ploog, Solid State Commun. **92**, 325 (1994).

[10] W. Langbein and J. M. Hvam, Phys. Rev. B **59**, 15405 (1999).

[11] F. M. Peeters, C. Riva, and K. Varga, Physica B **300**, 139 (2001).

[12] D. M. Whittaker and A. J. Shields, Phys. Rev. B **56**, 15185 (1997).

[13] C. Riva, F. M. Peeters, and K. Varga, Phys. Rev. B **63**, 115302 (2001).

[14] C. Riva, F. M. Peeters, and K. Varga, Phys. Rev. B **61**, 13873 (2000).

[15] A. Esser, E. Runge, R. Zimmermann, and W. Langbein, Phys. Rev. B **62**, 8232 (2000).

[16] T. Tsuchiya and S. Katayama, *Proceedings of the 24th International Conference on the Physics of Semiconductors, Jerusalem, 1998*, edited by D. Gershoni (World Scientific, Singapore, 1999).

[17] B. Stébé and A. Moradi, Phys. Rev. B **61**, 2888 (2000).

[18] G. Eytan, Y. Yayon, M. Rappaport, H. Shtrikman, and I. Bar-Joseph, Phys. Rev. Lett. **81**, 1666 (1998).

[19] J. G. Tischler, A. S. Bracker, D. Gammon, and D. Park, Phys. Rev. B **66**, 081310(R) (2002).

[20] G. Bastard, C. Delalande, M. H. Meynadier, P. M. Frijlink, and M. Voos, Phys. Rev. B **29**, 7042 (1984).

[21] O. Heller, Ph. Lelong, and G. Bastard, Phys. Rev. B **56**, 4702 (1997).

[22] L. C. O. Dacal, R. Ferreira, G. Bastard, and J. A. Brum, Phys. Rev. B **65**, 115324 (2002).

[23] L. C. O. Dacal, R. Ferreira, G. Bastard, and J. A. Brum, Phys. Rev. B **65**, 115325 (2002).

[24] A. Filinov, M. Bonitz, and Yu. E. Lozovik, Phys. Status Solidi C **238**, 1441 (2003); *Progress in Nonequilibrium Green's Functions II*, edited by M. Bonitz and D. Semkat (World Scientific, Singapore, 2003), p. 436.

[25] R. P. Feynman and A. R. Hibbs, *Quantum Mechanics and Path Integrals* (McGraw-Hill, New York, 1965).

[26] R. Winkler, Phys. Rev. B **51**, 14395 (1995).

[27] R. G. Storer, J. Math. Phys. **9**, 964 (1968); A. D. Klemm and R. G. Storer, Aust. J. Phys. **26**, 43 (1973).

[28] D. M. Ceperley, Rev. Mod. Phys. **65**, 279 (1995).

[29] A. S. Bracker *et al.* (private communication).

[30] C. Riva, F. M. Peeters, and K. Varga, Phys. Rev. B **64**, 235301 (2001).